Surface and Coatings Technology 183 (2004) 174–183

Structure and properties of reactive DC magnetron sputtered TiN/NbN hard superlattices

Harish C. Barshilia, K.S. Rajam*

Surface Engineering Division, National Aerospace Laboratories, Post Bag No. 1779, Bangalore 560 017, India

Received 10 March 2003; accepted in revised form 26 September 2003

Abstract

Nanostructured TiN/NbN superlattices at various modulation wavelengths (Λ) were deposited on silicon (111) and tool steel substrates using a reactive DC magnetron sputtering process. Structural characterization of the coatings was done using X-ray diffraction (XRD) in Bragg-Brentano θ–2θ geometry. All the multilayer coatings exhibited (111) preferred orientation in the XRD data. Appearance of satellite reflections (SR) along (111) principal reflection (PR) was used to check the quality of the superlattice coatings. The coatings exhibited superlattice structure for 106 Å $\geq \Lambda \geq$ 30 Å. The mechanical properties of the coatings were measured using a nanoindentation technique. The multilayer coatings exhibited hardness as high as 4000 kg/mm^2 at a modulation wavelength of 48 Å, which was $\sim$2.4 times the value of the rule-of-mixture. Thermal stability of the TiN/NbN multilayer coating was studied by vacuum annealing the coating for 30 min in the temperature range of 100–850 °C. Subsequent structural changes in the coating were measured by an in situ high-temperature X-ray diffractometer. Coating exhibited thermal stability up to 700 °C and subsequently showed reduction in the superlattice character. The corrosion behavior of 1.5 μm thick single layer TiN and NbN, and multilayer TiN/NbN (Λ = 50 Å) coatings deposited on tool steel substrates were investigated using potentiodynamic polarization in 0.5 M NaCl and 0.5 M HCl solutions under non-deaerated conditions. The microstructural changes, as a result of corrosion, were investigated by atomic force microscopy (AFM). The results indicated that the multilayer coatings exhibited superior corrosion resistance as compared to the single layer coatings.

Keywords: TiN/NbN superlattices; Reactive DC magnetron sputtering; Structural characterization; Nanoindentation; Thermal stability; Corrosion behavior

1. Introduction

In recent years a number of multilayer coating systems have been investigated [1]. These include metal/metal, metal/ceramic and ceramic/ceramic multilayer systems. Nanostructured multilayer coatings of ceramic materials (especially those of transition metal nitrides) are an emerging class of superhard materials [2,3]. In these materials repeating layered structure of two different materials with nanometer-scale dimensions are deposited onto a surface. These nanostructured multilayer coatings are commonly known as superlattices. The thickness of each successive pair of layers is commonly known as modulation wavelength (Λ), which critically affects the properties of the superlattices. These materials exhibit exotic properties such as high hardness [4]. Unlike other superhard coatings (e.g. CVD diamond) the ceramic multilayer coatings are expected to be stable even at higher working temperatures [5]. In principle, these coatings can be deposited (at low temperature) on any of the important engineering substrates with improved adhesion [6]. Superlattice coatings are not only technologically important but also very important scientific issues related to the enhancement in their properties need to be addressed.

Of late, a variety of polycrystalline and single-crystalline nitride multilayers, such as TiN/NbN [7–10], TiN/VN [11], TiN/CrN [12], TiN/ZrN [13], etc. have been developed, mainly by sputtering processes. Some of these coatings exhibit hardness as high as 50 GPa (CVD diamond = 80–90 GPa). Nanostructured TiN/NbN multilayers are one of the emerging superhard coatings. This system has attracted greater interest

*Corresponding author. Tel.: +91-80-5086247; fax: +91-80-5210113.

E-mail address: rajam@css.cmmacs.ernet.in (K.S. Rajam).

0257-8972/04/$ - see front matter © 2003 Elsevier B.V. All rights reserved.
doi:10.1016/j.surfcoat.2003.09.070

because of its good thermal expansion match with widely used tool steel/high-speed steel [14]. Due to the great similarities in properties like melting point, crystal structure and large difference in the hardness, TiN and NbN are being increasingly used to deposit isostructural superlattice coatings.

One of the possible uses of TiN/NbN multilayers is as hard protective coatings on cutting tools, which are exposed to high temperature during cutting process [15]. This application demands higher thermal stability as well as higher hardness of the coating. The thermal behavior of the multilayer coating is affected by the presence of interfaces as compared to the single layer coatings. Interdiffusion becomes one of the important factors in deciding the mechanical properties of the multilayer coatings at higher temperature [5]. Although, transition metal nitride coatings prepared by physical vapor deposition (PVD) are generally inert, the presence of a large number of pores and columnar structure degrades the corrosion behavior of the coatings significantly [16]. The corrosion behavior of PVD TiN and CrN coatings are fairly well documented in the literature but the corrosion behavior of NbN and multilayer coatings is not studied extensively. In general, it has been reported that multilayers exhibit superior corrosion resistance than single layer coatings [17–19].

In this paper, deposition and characterization of TiN/NbN superlattice coatings is described. X-Ray diffraction (XRD) has been used to study the structural properties of the coatings. The mechanical properties of the coatings have been studied using a nanoindentation technique. Thermal stability of the coatings has been studied using a high temperature X-ray diffractometer. Potentiodynamic polarization has been used to study the corrosion behavior of the coatings.

2. Experimental details

Alternate layers of TiN and NbN of varying thicknesses were deposited on silicon (111) and tool steel substrates using a reactive DC planar magnetron sputtering system that has been described in detail elsewhere [20]. The sputtering system consisted of 4 sputtering guns (3 inches in diameter). In order to get varying thicknesses of TiN and NbN layers, 6-mm thick high purity Ti (99.95%) and Nb (99.99%) targets were sputtered for different durations in high purity Ar (99.999%) and N_2 (99.999%) plasma. Typically, TiN/NbN multilayers were deposited under a base pressure of $\sim 2.0\times10^{-6}$ mbar and a total $Ar+N_2$ gas pressure of $\sim 4.0\times10^{-3}$ mbar. The flow rates of N_2 (1.5 sccm) and Ar (17 sccm) were controlled separately by MKS (model 247) mass flow controllers. Special gas feeding system was designed to create differential partial pressures of the reactive gas near the Nb and Ti targets. The substrate to target distance was 5.4 cm. A DC substrate bias (V_B) of -200 V was applied to improve the mechanical properties of the coatings. This resulted in ion current densities of 1.15 and 0.53 mA/cm^2 for TiN and NbN sputtered layers, respectively. For all the experiments, the power densities were $\sim$5.4 and $\sim$2.26 W/cm^2 for Ti and Nb targets, respectively. Under these conditions the growth rates were $\sim$2 Å/s each for TiN and NbN. The coatings were deposited at a substrate temperature of 400 °C. Multilayer coatings were obtained by a computer operated substrate rotation assembly, which controlled the dwell time of the substrate underneath each target very precisely. The total thicknesses of the films were $\sim$2.0 μm. The individual layer thicknesses of TiN and NbN were same for all the multilayers. Substrates were cleaned in ultrasonic bath using acetone, ethyl alcohol and trichloroethylene. Further cleaning was done by in situ Ar^+ ion bombardment, wherein a DC bias of -850 V was applied to the substrate for 30 min prior to the film deposition. Sputter cleaning of the targets was done for 15 min prior to the deposition. A 0.5 μm thick Ti interlayer was incorporated between the substrate and the film for improved adhesion. Table 1 summarizes the process conditions used for depositing TiN/NbN superlattices.

Table 1
Summary of deposition parameters

Target to substrate distance (cm)	5.4
Ti and Nb targets diameter (cm)	7.5
Initial vacuum (mbar)	$\sim 2.0\times10^{-6}$
Working pressure (mbar)	$\sim 4.0\times10^{-3}$
Nitrogen flow rate (sccm)	1.5
Argon flow rate (sccm)	17
N_2 flow near Nb target/N_2 flow near Ti target	$\sim$1.5
Power density on Ti target (W/cm^2)	5.40
Power density on Nb target (W/cm^2)	2.26
Substrate bias (V)	-200
Ion current density on TiN film (mA/cm^2)	1.15
Ion current density on NbN film (mA/cm^2)	0.53
Growth rate for TiN (Å/s)	$\sim$2
Growth rate for NbN (Å/s)	$\sim$2
Substrate temperature (°C)	400
Total thickness of the coating (μm)	2

The XRD data of the films in Bragg–Brentano θ–2θ geometry were recorded in a Rigaku D/max 2200 Ultima X-ray powder diffractometer. The X-ray source was a Cu Kα radiation ($\lambda = 1.5418$ Å), which was operated at 40 kV and 40 mA. The spectra were recorded in the angular range of $50^\circ \geq 2\theta \geq 30^\circ$ with very slow scan speed (0.25° per minute). Spectra were also recorded at $60^\circ \leq 2\theta \leq 65^\circ$, $70^\circ \leq 2\theta \leq 76^\circ$, $75^\circ \leq 2\theta \leq 80^\circ$, $90^\circ \leq 2\theta \leq 96^\circ$ and $101^\circ \leq 2\theta \leq 106^\circ$ to find out the intensities of (220), (311), (222), (400) and (331) reflections, respectively. High temperature XRD measurements were taken in a 1.2 kW Siemens Kristalloflex diffractometer (Cu Kα radiation) in Bragg–Brentano θ–2θ geometry. The high temperature attachment was

operated under a vacuum of $\sim 2.0\times10^{-6}$ mbar. The data were recorded in the temperature range (T_a) of 100–850 °C at an interval of 50 °C. The heating rate was 0.2 °C per minute. Before recording the XRD data, the sample was kept at the desired temperature for 30 min. The data collection time was 15 s for a step size of 0.05°.

The hardness measurements were performed in a nanoindenter (CSEM Instruments) at a load of 5 mN using a Berkovich diamond indenter. At this load the indentation depth was much less than 1/10th of the coating thickness, thus eliminating the effect of substrate on the hardness measurements. For nanoindentation measurements, the samples were polished with 0.03 μm alumina powder to reduce the surface roughness. Ten indentations were made on each sample. The surface roughness of the coatings was studied using an atomic force microscope (AFM).

Corrosion studies were made in 0.5 M NaCl and 0.5 M HCl solutions (nondeaerated) using a potentiodynamic polarization unit consisting of three electrodes. One of the electrodes (area = 1 cm^2) served as the working electrode and a platinum electrode served as the counter electrode, which was kept parallel to the working electrode. A saturated calomel electrode (SCE) with a luggin capillary acted as the reference electrode. This electrode was kept near the surface of the working electrode and measured the potential of the working electrode. The samples were immersed in the solution for about half an hour so that a steady equilibrium potential, known as open circuit potential (OCP), was attained. The polarization of the samples was carried out, first cathodically and then anodically by approximately ±150 mV above the OCP to cover the Tafel region (±60 to ±120 mV) of the polarization. Current and potential were recorded simultaneously. Tafel plots were made from the data and the corrosion current density was determined by extrapolating the straight-line section of the anodic and cathodic Tafel lines [21].

3. Results and discussion

3.1. Structure of TiN/NbN superlattices

In a reactive magnetron sputtering process the structure of TiN and NbN coatings depends strongly on the nitrogen partial pressure, the sputtering yield and the substrate bias. Transition metal nitrides exist in different stoichiometric phases [22]. For example, NbN may occur in following phases: β-Nb_2N, γ-NbN_x and δ-NbN. δ-NbN has a cubic B1 NaCl fcc structure with a lattice parameter of 4.4100 Å. There is a limited range of nitrogen concentration, wherein stoichiometric phases of TiN (38–50 at.% nitrogen) and δ-NbN (42–46 at.% nitrogen) with B1 structure exist [22–24]. As the heats of formation of TiN (−80.8 kcal/mol) and NbN (−56.2 kcal/mol) differ significantly [25], simultaneous deposition of TiN and NbN coatings in a reactive sputtering process is difficult. In order to do so, partial pressures of nitrogen have to be controlled judiciously near Ti and Nb targets. Considering all the above points, it becomes essential first to optimize the process parameters for the deposition of cubic TiN and NbN phases with B1 structure. The deposition conditions were carefully optimized after a series of experiments involving variations of nitrogen partial pressure, sputtering power, substrate bias, operating pressure, etc. Process parameters listed in Table 1 resulted in a single phase TiN and NbN coatings. Typical XRD data of TiN, NbN and TiN/NbN coatings deposited under the above deposition conditions are presented in Fig. 1. The lower panels of Fig. 1 show the XRD data of TiN and NbN coatings with a prominent reflection along (111) plane. The intensity of (200) reflection for both TiN and NbN was very low. Other reflection planes such as (220) and (311) are completely absent in the diffraction patterns (not plotted in the figure). This showed that under these deposition conditions both TiN and NbN coatings were preferentially oriented along (111) plane. After optimizing the deposition conditions for TiN and NbN, multilayer coatings of TiN/NbN were prepared. The top panel of Fig. 1 shows a typical XRD pattern of TiN/NbN multilayer coating deposited at a modulation wavelength of 48 Å. For the multilayer, the structure was composed of a principal reflection (PR), the d value (2.5370 Å) of which was in between that of TiN (2.4840 Å) and NbN (2.5481 Å). The principal reflection was flanked by 1st order negative satellite reflection (SR),

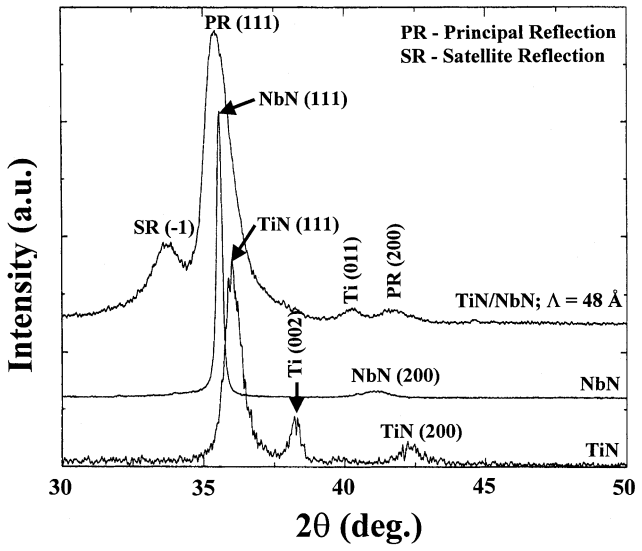

Fig. 1. XRD patterns of: (a) a single layer TiN coating (b) a single layer NbN coating and (c) a TiN/NbN multilayer coating with a modulation wavelength of 48 Å.

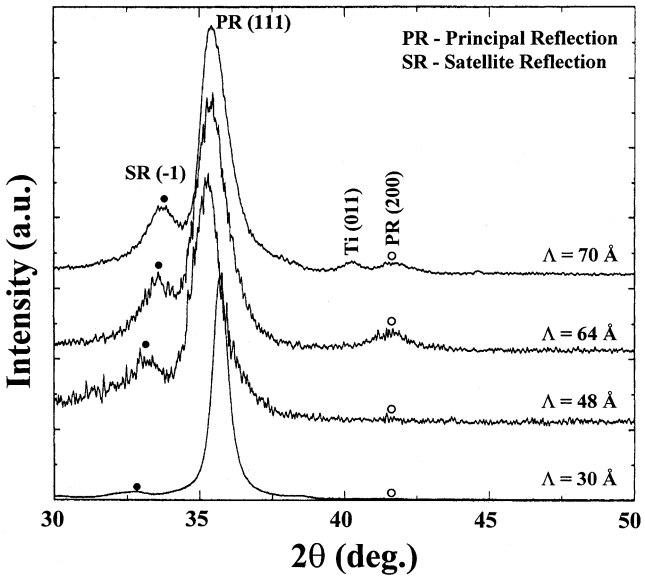

Fig. 2. XRD data of TiN/NbN multilayers with different modulation wavelengths. The spectra show (111) principal reflection, which is flanked by 1st order negative satellite reflection.

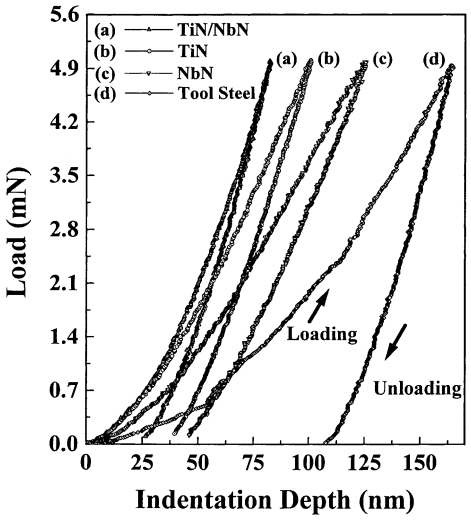

Fig. 3. Schematic representations of load vs. displacement curves at 5 mN load for (a) a TiN/NbN multilayer coating (b) a TiN coating (c) a NbN coating and (d) a tool steel substrate.

which was indicative of superlattice formation under these conditions.

The XRD data of TiN/NbN superlattices deposited at different modulation wavelengths are shown in Fig. 2. Superlattice structure was clearly seen for the films deposited at 106 Å $\geq \Lambda \geq$ 30 Å. Samples did not show prominent positive satellites, which was attributed to larger lattice spacing and higher X-ray scattering factor for NbN than TiN. At very low modulation wavelengths ($\Lambda < 30$ Å) only a broad principal reflection was observed and satellite reflections were absent, indicating that a long-range crystalline order was no longer maintained. Multilayer coatings with 106 Å $\geq \Lambda \geq$ 48 Å showed broader XRD peaks than TiN and NbN, which means that multilayers (approx. 110 Å) had smaller grain size than the single layer TiN (approx. 150 Å) and NbN (approx. 200 Å) coatings. The full width at half-maximum (FWHM) of the (111) peak decreased with an increase in the modulation wavelength, however, its position remained unaffected. A summary of the XRD data, for the samples studied in the present work, is listed in Table 2. As can be seen from the Table the 1st order negative satellite reflection moved closer to the principal reflection with an increase in Λ. The intensity ratio of 1st order negative satellite to the principal Bragg peak (I_{-1}/I_B) was maximum at $\Lambda = 64$ Å. It decreased markedly at low modulation wavelengths and at very low Λ the satellite reflections were completely absent. This signifies that there was a limited range of Λ, wherein superlattice formation was possible.

3.2. Mechanical properties of TiN/NbN superlattices

Load vs. displacement curves were measured for single layer TiN, single layer NbN, TiN/NbN multilayer coatings and tool steel substrate at 5 mN load. Typical plots obtained for four samples are shown in Fig. 3. After initial contact of the indenter on the surface, the

Table 2
X-Ray diffraction data of the films studied in the present work

Coating	Modulation wavelength (Å)	Total number of layers	Preferred orientation	Structure	(111) Peak position ($2\theta°$)	FWHM of (111) peak ($2\theta°$)	I_{-1}/I_B	1st Order (−ve) satellite reflection position ($2\theta°$)
TiN	–	–	{111}	B1 NaCl fcc	36.16	0.586	–	–
NbN	–	–	{111}	B1 NaCl fcc	35.22	0.556	–	–
Multilayer	106	376	{111}	B1 NaCl fcc	35.26	0.840	0.260	33.98
Multilayer	80	500	{111}	B1 NaCl fcc	35.26	0.890	0.320	33.86
Multilayer	70	570	{111}	B1 NaCl fcc	35.32	0.980	0.324	33.16
Multilayer	64	624	{111}	B1 NaCl fcc	35.38	1.012	0.360	33.02
Multilayer	48	770	{111}	B1 NaCl fcc	35.40	1.220	0.240	32.80
Multilayer	30	1334	{111}	B1 NaCl fcc	35.64	0.900	0.040	32.68

load was increased at a predetermined rate (10 mN/min) to the desired maximum load (5 mN) and then decreased at the same rate (10 mN/min) to zero. The unloading curve followed the partial elastic recovery of the sample material. From this plot the hardness was calculated using Oliver and Pharr method [26]. The area formed by the loading and the unloading curves, defined as plastic deformation work, can be used to assess the resistance of plastic deformation and the wear resistance of the coatings [27]. The resistance of plastic deformation is inversely proportional to the plastic deformation work. In the present study, TiN/NbN multilayer coatings showed the smallest plastic deformation work and the largest resistance to plastic deformation as compared to the single layer TiN and NbN coatings. For the softest film (i.e. NbN), the maximum indentation depth was 120 nm, which was much less than 1/10th of the coating thickness, thus eliminating the effect of substrate on the hardness measurements. Tool steel substrate showed a maximum indentation depth of 160 nm. For the hardest film (i.e. TiN/NbN), however, the maximum indentation depth was only 85 nm. It must be mentioned here that all the nanoindentation measurements were largely unaffected by surface roughness of the coatings. The root-mean-square (rms) surface roughness, R_a, of TiN, NbN and TiN/NbN multilayers, with a total thickness of 2.0 μm, was investigated by AFM. Typical rms roughness values for TiN, NbN and TiN/NbN were 6.04 nm, 2.89 nm and 5.49 nm, respectively. The nanoindentation data were also corrected for indenter size effect.

The variation of nanoindentation hardness of TiN/NbN multilayers with modulation wavelength is shown in Fig. 4. The peak hardness occurred at $\Lambda = 48$ Å and the maximum hardness obtained was ~4000 kg/mm^2, which was nearing to that of a superhard material. The hardness values of TiN, NbN coatings and tool steel substrate were ~2000 kg/mm^2, 1400 kg/mm^2 and 1100 kg/mm^2, respectively. The maximum hardness obtained was much higher than the value of the rule-of-mixture, which for TiN–NbN is ~1700 kg/mm^2. For the multilayer coatings pronounced variations in the strength and hardness as a function of modulation wavelength are commonly observed [7–13,20]. For example, TiN/NbN multilayers exhibit hardness varying from 3600 to 5000 kg/mm^2 depending on the deposition process and the growth conditions. Similarly, Cu/Ni multilayers show a hardness enhancement by a factor of ~2.4 times the value of the rule-of-mixture [20]. Apart from the modulation wavelength, hardness of the coatings was also dependent on the substrate bias. A maximum hardness of 4000 kg/mm^2 ($\Lambda = 48$ Å) was achieved at $V_B = -200$ V. The hardness decreased from 4000 to 3300 kg/mm^2 as the bias was decreased from −200 to −150 V. At very high substrate bias (e.g. $V_B \geq -225$ V) the hardness again decreased, presumably because

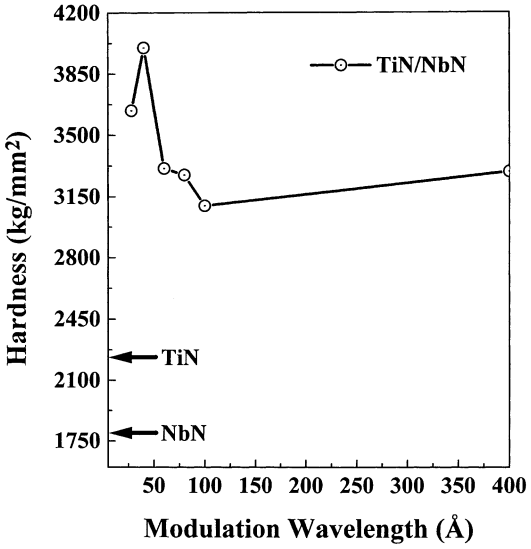

Fig. 4. Variation of nanoindentation hardness of TiN/NbN multilayer coatings with modulation wavelength. Also, shown are the hardnesses of single layer TiN and single layer NbN coatings.

of ion beam intermixing effects at the interfaces and interface roughening. This observation is consistent with the earlier reports on effect of bias on the mechanical properties of TiN/NbN superlattices [8,14]. The enhanced hardness can be explained by ion-induced densification below −200 V and deterioration of the superlattice structure caused by interdiffusion and interface roughness above −200 V.

A variety of mechanisms have been put forward to explain the hardness enhancement in the multilayer superlattice coatings. These include suppression of dislocations (Koehler strengthening), grain refinement (Hall–Petch), coherency strain hardening, dislocation line energy effects and interfacial crack deflection [3,28,29]. In general, enhancement in the hardness results from the resistance to dislocation glide across the interfaces, which is proportional to the difference in the layer shear moduli. The observed enhancement in the hardness in TiN/NbN multilayer samples at low modulation wavelength (40–108 Å) is primarily believed to be due to the interfaces. At low modulation wavelengths, the interfaces between the layers act as pinning sites for dislocations. As the thicknesses of TiN and NbN layers are too small, the dislocation generation (such as Frank Read) cannot occur inside the layers. Even if the dislocations are generated in the layers they propagate towards the interfaces. As the interfacial energies are quite high, further movement of the dislocations is prevented and hence pile-up of the dislocations takes place near the interfaces. Furthermore, each interface serves as crack-tip deflectors. This leads to a substantial increase in the system hardness relative to that of the homogeneous materials. However, the same

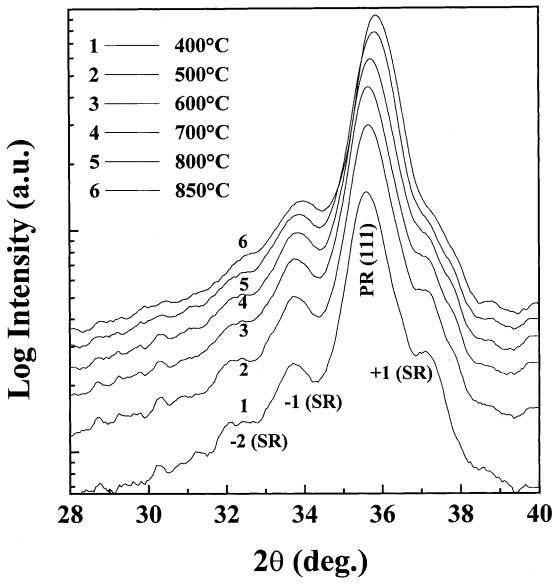

Fig. 5. High-temperature XRD data of a TiN/NbN superlattice coating annealed at 400, 500, 600, 700, 800 and 850 °C. The modulation wavelength was 50 Å.

arguments are not true at very low modulation wavelengths, where the multilayer behaves like an alloy. At large modulation wavelengths, softening occurs as a result of dislocation motions within the individual layers. It must be mentioned that the maximum enhancement in the hardness of a superlattice coating also depends on the microstructure and stress level of the coating, irrespective of the modulation wavelength.

3.3. Thermal stability of TiN/NbN superlattices

TiN/NbN ($\Lambda = 50$ Å) multilayer coating deposited on silicon substrate was annealed at 100–850 °C for 30 min. The maximum annealing temperature was well below the melting point of TiN (2950 °C) and NbN (2300 °C). Typical high temperature XRD plots obtained from a TiN/NbN multilayer sample annealed at 400, 500, 600, 700, 800 and 850 °C are shown in Fig. 5. All the plots exhibited strong (111) principal reflection. First and 2nd order negative satellites and 1st order positive satellite were seen along the (111) principal peak. The XRD data were deconvoluted using a Peak-Fit program to calculate the peak position, the peak intensity and the FWHM of the principal and the satellite reflections. These results are plotted in Fig. 6. As shown in Fig. 6a, the position of the (111) principal reflection shifts to higher 2θ values. This may be attributed to stress relaxation as a result of annealing. Compressive stresses are commonly observed in bias sputtered films and can be explained by the increase in point defects created by Ar^+ ion bombardment [30]. The FWHM of (111) peak decreases with T_a and this decrease is significant for $T_a > 700$ °C. The average crystallite size, as calculated from the FWHM of (111) peak, increased from 97 to 179 Å as the annealing temperature increased from 100 to 850 °C. The grain growth actually occurred for $T_a > 700$ °C, as evidenced by a significant sharpening of (111) peak above this temperature.

The normalized intensity (I_{-1}/I_B) and FWHM of 1st order negative satellite reflection, for example, can be used to determine the quality of the superlattice coating after annealing [31]. Variations of (I_{-1}/I_B) and FWHM of the SR peak with annealing temperature are plotted in Fig. 6b. No significant change in I_{-1}/I_B was observed up to 700 °C, however, it decreased significantly for $T_a > 700$ °C. Similarly, FWHM of the SR peak increased considerably for $T_a \geq 700$ °C. Both these observations

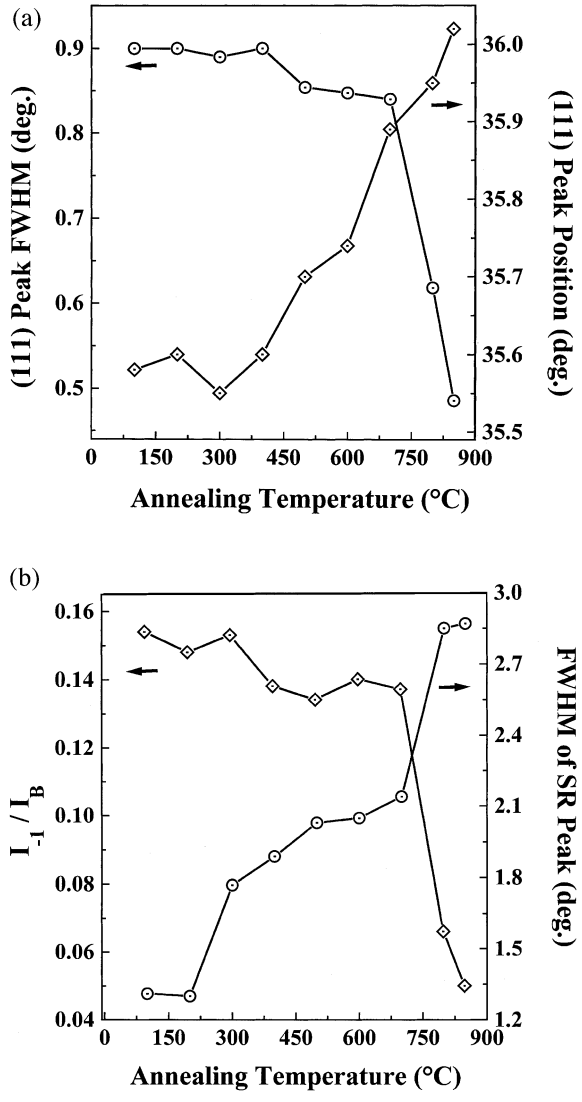

Fig. 6. Variations of: (a) peak position and FWHM of principal reflection, and (b) FWHM and normalized intensity of 1st order negative satellite reflection of a TiN/NbN multilayer coating ($\Lambda = 50$ Å), with annealing temperature.

indicate that the coating perfectly retained its superlattice character up to 700 °C and subsequently started degrading marginally. The position of the satellite reflection did not change with annealing temperature, indicating no change in the modulation wavelength. Hence, variations in the layer thicknesses were minimal during annealing.

Annealing of a multilayer coating can lead to the following microstructural changes: (i) interdiffusion (ii) coarsening of the layers (iii) reactions between the layers to produce a new phase and (iv) transformation within one or both layers [5]. It has been reported by Hultman et al. [31,32] that single-crystalline TiN/NbN superlattices exhibit a non-linear diffusion with different activation energies in the different temperature regimes. For example, activation energies of 1.2, 2.6 and 4.5 eV have been reported for $T_a \leq 830$ °C, 875 °C $\geq T_a \geq 830$ °C and 930 °C $\geq T_a \geq 875$ °C, respectively. The lower activation energy was attributed to defect-mediated diffusion, whereas, the higher activation energies were attributed to bulk diffusion. The different activation energies have been attributed to shift in relative layer thicknesses and different diffusion rates of Ti in NbN (fast) and Nb in TiN (slow). Lopez et al. also observed that annealing of TiN/NbN multilayers caused almost no intermixing up to 700 °C, while the hardness, the adhesion/cohesion, and the structure remained unaffected [33]. Present high temperature XRD data also support a non-linear diffusion in TiN/NbN superlattices. Further, it is demonstrated that TiN/NbN multilayer coatings retained superlattice structure even up to 850 °C and none of the four microstructural changes, as discussed above, were significantly operational for $T_a \leq 700$ °C. The diffusion behavior of the polycrystalline multilayer coatings, in fact, depends on the factors like variations in exact composition and growth-induced defect density [32]. Nevertheless, it appears that the polycrystalline TiN/NbN superlattices exhibit similar diffusion behavior as that of the single crystalline superlattices.

3.4. Corrosion behavior of TiN/NbN superlattices

The potentiodynamic polarization curves obtained for tool steel substrate, single layer NbN, single layer TiN and multilayer TiN/NbN ($\Lambda = 50$ Å) coatings in non-deaerated 0.5 M NaCl solution are shown in Fig. 7a. The thickness and the area of the coating were 1.5 μm and 6.25 cm^2, respectively, for all the samples. The multilayer coating had 600 interfaces. The corrosion potential relative to SCE (E_{corr}) and corrosion current density (I_{corr}) obtained from these plots are presented in Table 3. After coating the substrate with 1.5 μm thick TiN/NbN multilayer, E_{corr} increased from -0.505 to -0.355 V, thus indicating more noble behavior. The corresponding I_{corr} values were 9.6 μA/cm^2 and 0.9 μA/cm^2, respectively. Single layer TiN and NbN coatings exhibited almost similar corrosion behavior. A

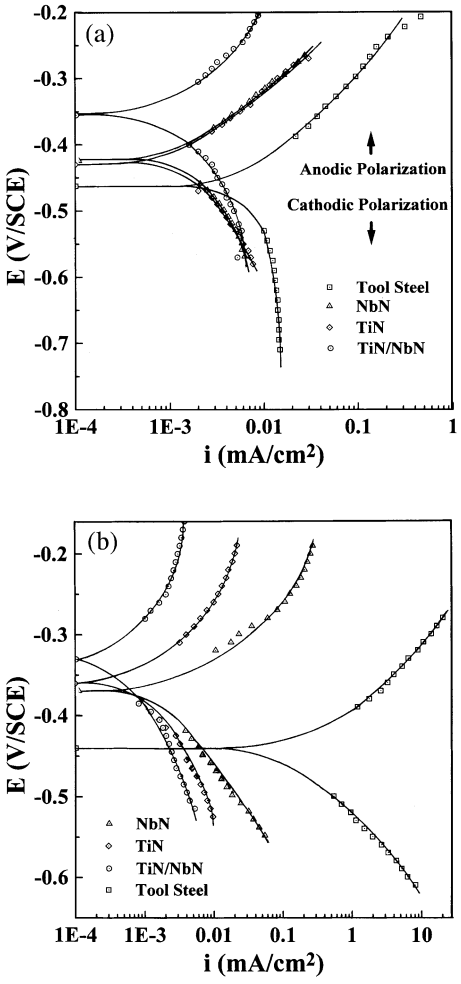

Fig. 7. Potentiodynamic polarization curves of a single layer TiN coating, a single layer NbN coating, a TiN/NbN multilayer ($\Lambda = 50$ Å) coating and a tool steel substrate in non-deaerated conditions in (a) 0.5 M NaCl and (b) 0.5 M HCl solutions.

small, but significant, increase in E_{corr} (approx. 65 mV) for multilayer coating as compared to the single layer TiN and NbN coatings may suggest that the multilayer coating was more noble than single layer. Corrosion characteristics of the samples in non-deaerated 0.5 M HCl solution are shown in Fig. 7b. In this case, also, E_{corr} increased from -0.460 to -0.325 V after coating the substrate with 1.5-μm thick TiN/NbN multilayer. However in this case, I_{corr} for tool steel substrate was very high (240 μA/cm^2) as compared to 0.82 μA/cm^2 for multilayer coating. Thus, the multilayer coating exhibited a 290-fold decrease in I_{corr} as compared to the bare substrate. The fact that all the three coatings, studied in present work, behaved more or less same in both HCl (more aggressive) and NaCl solutions indicate that porosity was minimal. Considering the low thicknesses of the samples studied in the present work (1.5 μm), the good corrosion resistance is believed to be due to a denser microstructure of the coatings, resulting

Table 3
Corrosion characteristics of tool steel, single layer TiN, single layer NbN and multilayer TiN/NbN coatings in 0.5 M NaCl and 0.5 M HCl solutions

Sample	0.5 M NaCl		0.5 M HCl	
	E_{corr} (V vs. SCE)	I_{corr} ($\mu A/cm^2$)	E_{corr} (V vs. SCE)	I_{corr} ($\mu A/cm^2$)
Tool Steel	−0.505	9.6	−0.460	240
TiN	−0.420	1.5	−0.365	1.1
NbN	−0.420	1.3	−0.375	1.6
TiN/NbN	−0.355	0.9	−0.325	0.82

from the increased ion bombardment during the deposition. This was confirmed by AFM images.

The microstructural changes as a result of corrosion were investigated by AFM and representative three-dimensional morphologies are presented in Fig. 8. Uncoated substrate exhibited very smooth surface morphology with an rms roughness of 4.6 nm. After corrosion in 0.5 M HCl solution the substrate became very rough and R_a increased to 266 nm. Substrate coated with TiN/NbN multilayer exhibited an rms roughness of 5.2 nm and it did not change even after corrosion in 0.5 M HCl solution (5.4 nm after corrosion). Similarly, no significant change in the microstructure of the single layer TiN and NbN coatings was observed after corrosion.

In general, transition metal nitride coatings are relatively inert to the chemical attacks due to their relatively higher position in the electrochemical series. As these

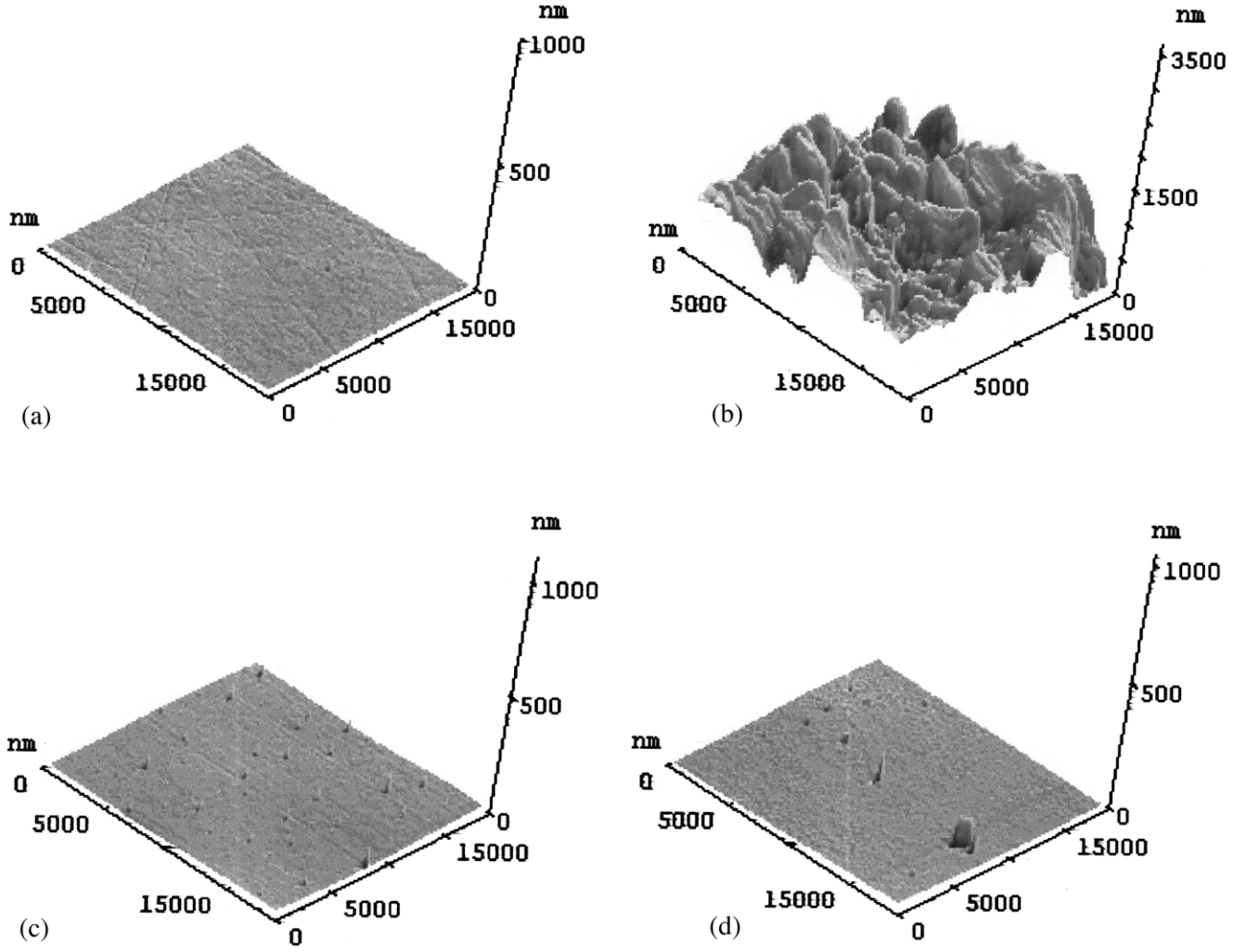

Fig. 8. Three-dimensional AFM morphologies of: (a) and (b) tool steel substrate before and after corrosion, (c) and (d) TiN/NbN multilayer on tool steel substrate before and after corrosion in 0.5 M HCl solution.

coatings are prepared by PVD techniques, which generally lead to porosity/defects in the coatings during deposition. These pores act as primary source of corrosion. In fact, presence of pores can easily be detected by corrosion measurements. Adhesion is another issue, which affects the corrosion characteristic of a coating significantly. If adhesion of the coating on the substrate is not good, the production of gas bubbles during the corrosion test can delaminate large coating areas, which subsequently degrades the corrosion behavior of the coating [34,35]. Of course, the corrosion behavior of thin coatings depends on the thickness of the coatings. For example, Lang and Yu reported an excellent corrosion resistance of TiN coatings having thicknesses of 12 and 18 μm [36]. However, at lower thicknesses (i.e. ≤ 6 μm), the corrosion resistance was very poor. This was attributed to higher defects and or pores at lower coating thicknesses. Very limited studies on the corrosion of multilayers are reported in the literature [17–19,34–40] and it has been shown that the corrosion behavior of multilayers is largely modified by the presence of a large number of interfaces. For example, superior corrosion behavior of TiN/CrN multilayer coatings as compared to the single layer coatings has been reported by Nordin et al. [19]. Ries et al. [39] have shown that the corrosion resistance of multilayer coating depends on the nature of interface. They reported that the corrosion resistance can be more effectively increased by using graded interface coatings instead of sharp interface coatings. The better performance of the graded interface coating has been related to the reduced interfacial stresses. In the present work, the multilayer coatings showed better corrosion behavior as compared to the single layer coatings but this improvement was not very significant. For example, in 0.5 M HCl solution, I_{corr} for TiN and TiN/NbN coatings were 1.1 and 0.82 μA/cm^2, respectively. The corresponding E_{corr} values were -0.365 and -0.325 V. Given the fact that multilayers contained as many as 600 interfaces, there should be other factors, apart from the interfaces, which control the corrosion behavior of multilayer coatings. Clearly, more work is needed to understand the exact mechanism of corrosion in multilayer coatings.

4. Conclusions

A reactive DC magnetron sputtering system was used to deposit nanostructured TiN/NbN multilayer coatings on silicon and high-speed steel substrates at various modulation wavelengths. Judicious control of the process parameters resulted in the deposition of polycrystalline TiN/NbN multilayer coatings with B1 NaCl fcc structure. All the coatings exhibited preferred orientation along (111) plane. The X-ray diffraction data showed that the coatings exhibited a superlattice structure for a modulation wavelength such that 30 Å $\leq \Lambda \leq$ 106 Å. The position of 1st order negative satellite shifted to higher 2θ value with an increase in Λ. The intensity of satellite reflection was maximum at $\Lambda = 64$ Å and reduced to zero for $\Lambda < 30$ Å. This has been attributed to alloying at low modulation wavelengths. Nanoindentation data showed that for the films prepared at $\Lambda = 48$ Å and $V_B = -200$ V the hardness was as high as 4000 kg/mm^2, which was approximately ~ 2.4 times the rule-of-mixtures value. High-temperature XRD data of the annealed TiN/NbN multilayer showed that the coating retained its superlattice structure up to 700 °C and indicated a degradation in the quality of the coating for $T_a > 700$ °C. This was attributed to interdiffusion in the coating at higher temperatures. The multilayer coatings exhibited a 290-fold decrease in I_{corr} as compared to the uncoated steel substrate in 0.5 M HCl solution. Similarly, in 0.5 M NaCl solution the multilayer coatings exhibited superior corrosion resistance as compared to the bare substrate. No significant microstructural changes were observed in AFM as result of corrosion of TiN/NbN multilayers. The present work shows that TiN/NbN superlattices not only possess superior mechanical properties but also superior thermal and chemical properties.

Acknowledgments

The authors thank Director, NAL for giving permission to publish these results. Thanks are due to Dr Anjana Jain for XRD measurements and Mr A. Poojari for potentiodynamic polarization measurements. Authors also thank Dr Sharat Chandra for high temperature XRD measurements. This research was supported by the Department of Science and Technology, New Delhi and the Council of Scientific and Industrial Research, New Delhi, India.

References

[1] S. Barnett, A. Madan, Phys. World (1998) 45.
[2] W.D. Sproul, Science 273 (1996) 889.
[3] P.C. Yashar, W.D. Sproul, Vacuum 55 (1999) 179.
[4] J. Musil, Surf. Coat. Technol. 125 (2000) 322.
[5] L. Hultman, Vacuum 57 (2000) 1.
[6] P.E. Hovsepian, D.B. Lewis, W.D. Munz, Surf. Coat. Technol. 133–134 (2000) 166.
[7] X. Chu, S.A. Barnett, M.S. Wong, W.D. Sproul, Surf. Coat. Technol. 57 (1993) 13.
[8] X. Chu, M.S. Wong, W.D. Sproul, S.L. Rohde, S.A. Barnett, J. Vac. Sci. Technol. A 10 (1992) 1604.
[9] M. Shinn, L. Hultman, S.A. Barnett, J. Mater. Res. 7 (1992) 901.
[10] M. Larsson, M. Bromark, P. Hedenqvist, S. Hogmark, Surf. Coat. Technol. 91 (1997) 43.
[11] U. Helmersson, S. Todorova, S.A. Barnett, J.E. Sundgren, L.C. Markert, J.E. Greene, J. Appl. Phys. 62 (1987) 481.
[12] M. Nordin, M. Larsson, S. Hogmark, Wear 232 (1999) 221.

[13] I. Wadsworth, D.B. Lewis, G. Williams, J. Mater. Sci. 31 (1996) 5907.
[14] H. Ljungcrantz, E. Engstrom, L. Hultman, M. Olsson, X. Chu, M.S. Wong, W.D. Sproul, J. Vac. Sci. Technol. A 16 (1998) 3104.
[15] T.I. Selinder, M.E. Sjostrand, M. Nordin, M. Larsson, A. Ostlund, S. Hogmark, Surf. Coat. Technol. 105 (1998) 51.
[16] L. Cunha, M. Andritschky, L. Rebouta, K. Pischow, Surf. Coat. Technol. 116–119 (1999) 1152.
[17] E. Soderlund, P. Ljunggren, Surf. Coat. Technol. 110 (1998) 94.
[18] C. Liu, A. Leyland, Q. Bi, A. Matthews, Surf. Coat. Technol. 141 (2001) 164.
[19] M. Nordin, M. Herranen, S. Hogmark, Thin Solid Films 348 (1999) 202.
[20] H.C. Barshilia, K.S. Rajam, Surf. Coat. Technol. 155 (2002) 195.
[21] R. Greef, Instrumental Methods in Electrochemistry, Ellis Horwood, New York, 1990.
[22] L.E. Toth, Transition Metal Carbides and Nitrides, Academic Press, New York, 1971.
[23] K.S. Havey, J.S. Zabinski, S.D. Walck, Thin Solid Films 303 (1997) 238.
[24] H. Holleck, J. Vac. Sci. Technol. A 4 (1986) 2661.
[25] R.C. Weast, M.J. Astle (Eds.), CRC Handbook of Chemistry and Physics, 63rd ed, CRC Press, Inc, 1982.
[26] W.C. Oliver, G.M. Pharr, J. Mater. Res. 7 (1992) 1564.
[27] Y. Zhou, R. Asaki, W.H. Soe, R. Yamamoto, R. Chen, A. Iwabuchi, Wear 236 (1999) 159.
[28] S.A. Barnett, M. Shinn, Annu. Rev. Mater. Sci. 24 (1994) 481.
[29] X. Chu, S.A. Barnett, J. Appl. Phys. 77 (1995) 4403.
[30] H. Ljungcrantz, L. Hultman, J.E. Sundgren, L. Karlsson, J. Appl. Phys. 78 (1995) 832.
[31] C. Engstrom, J. Birch, L. Hultman, C. Lavoie, C. Cabral, J.L. Jordan-Sweet, J.R.A. Carlsson, J. Vac. Sci. Technol. A. 17 (1999) 2920.
[32] L. Hultman, C. Engstrom, M. Oden, Surf. Coat. Technol. 133–134 (2000) 227.
[33] S. Lopez, M.S. Wong, W.D. Sproul, J. Vac. Sci. Technol. A 13 (1995) 1644.
[34] H.W. Wang, M.M. Stack, S.B. Lyon, P. Hovsepian, W.D. Munz, Surf. Coat. Technol. 126 (2000) 279.
[35] M. Fenker, M. Blazer, H.A. Jehn, H. Kappl, J.J. Lee, K.H. Lee, H.S. Park, Surf. Coat. Technol. 150 (2002) 101.
[36] F. Lang, Z. Yu, Surf. Coat. Technol. 145 (2001) 80.
[37] M. Tomlinson, S.B. Lyon, P. Hovsepian, W.D. Munz, Vacuum 53 (1999) 117.
[38] W.D. Munz, L.A. Donohue, P.E. Hovsepian, Surf. Coat. Technol. 125 (2000) 269.
[39] L.A.S. Ries, D.S. Azambuja, I.J.R. Baumvol, Surf. Coat. Technol. 89 (1997) 111.
[40] L. Cunha, M. Andritschky, K. Pischow, Z. Wang, A. Zarychta, A.S. Miranda, A.M. Cunha, Surf. Coat. Technol. 133–134 (2000) 61.